Collisional Perturbation of States in Atomic Ytterbium by Helium and Neon

D.F. Kimball[a], D. Clyde[a], D. Budker[a,b], D. DeMille[c], S.J. Freedman[a,b], S. Rochester[a], J.E. Stalnaker[a], and M. Zolotorev[d]

[a] *Physics Department, University of California, Berkeley, CA 94720-7300*

[b] *Nuclear Science Division, Lawrence Berkeley National Laboratory, Berkeley, CA 94720*

[c] *Physics Department, Yale University, New Haven, CT 06520*

[d] *Center for Beam Physics, Lawrence Berkeley National Laboratory, Berkeley, CA 94720*

Results of an investigation of collisional de-excitation of the metastable 6s6p $^3P_0$ state in atomic ytterbium by helium and neon buffer gases are reported. We find upper limits for the quenching cross sections to be $s_{He} < 13 \times 10^{-22}$ cm^2 and $s_{Ne} < 8 \times 10^{-22}$ cm^2. The small cross sections may allow an ytterbium parity nonconservation experiment to be performed in a vapor cell. We have also measured the pressure broadening and shift of the 6s6p $^3P_0 \rightarrow$ 6s7s $^3S_1$ and 6s^2 $^1S_0 \rightarrow$ 6s6p $^3P_1$ transitions by helium and neon.

PACS numbers: 34, 11.30.Er, 42.62.Fi

(Submitted to Phys. Rev. A)

1. INTRODUCTION

The 6s^2 $^1S_0 \rightarrow$ 6s5d $^3D_1$ transition in atomic ytterbium (Yb) was recently proposed as a candidate for the study of parity nonconservation (PNC) [1] (hereafter the upper and lower states of this transition will be referred to as $^1S_0$ and $^3D_1$, respectively). This transition is well suited for the PNC-Stark interference technique, with a relatively large predicted PNC-induced $E1$ amplitude ($E1_{PNC} \approx 10^{-9}\, ea_0$ [1-3]), moderate Stark-induced $E1$ amplitude (vector transition polarizability $|b| = 2.18(33) \times 10^{-8}\, ea_0/(\mathrm{V/cm})$ [4]) and small $M1$ amplitude [5]. Many of the Yb atoms (approximately 70% [6]) excited to the $^3D_1$ state subsequently decay to the metastable 6s6p $^3P_0$ state (hereafter referred to as $^3P_0$, Fig. 1). Since one-photon radiative decays from the $^3P_0$ state to the ground state

are strictly forbidden by the $J=0 \nleftrightarrow J'=0$ selection rule, the lifetime of the metastable state is limited primarily by collisional de-excitation (quenching). Thus, if the quenching rate is sufficiently small, an effective detection scheme for an Yb PNC experiment is possible by inferring the $^1S_0 \rightarrow {}^3D_1$ transition rate from the population of atoms which accumulate in the $^3P_0$ state. This population can be efficiently probed by measuring absorption of laser light tuned to the 649 nm $^3P_0 \rightarrow 6s7s\ ^3S_1$ (hereafter $^3S_1$) transition. This technique may enable an Yb PNC measurement to be performed in a vapor cell, offering a potential improvement in statistical sensitivity to PNC effects compared to an experiment performed with an atomic beam.

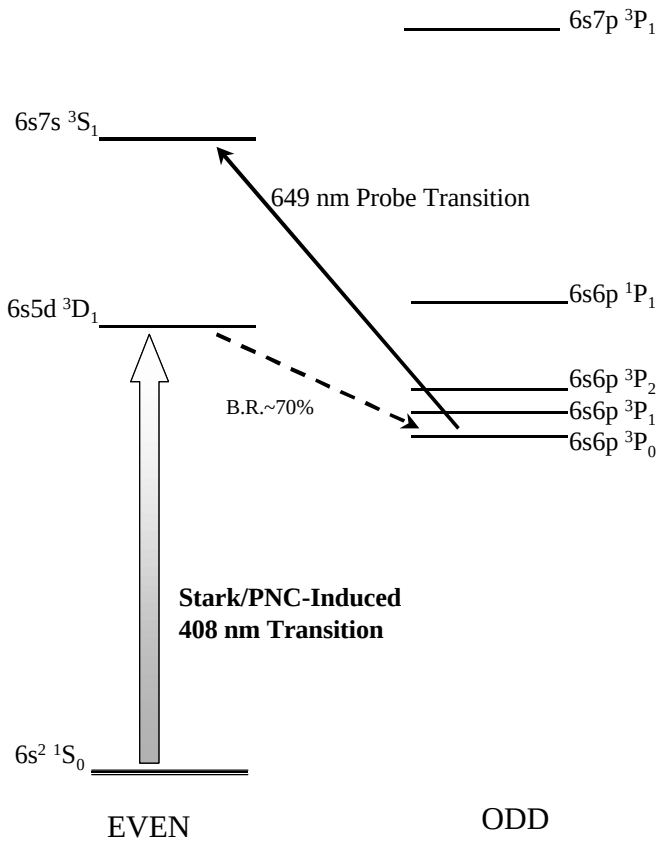

FIG. 1. *Partial energy level diagram of atomic ytterbium and relevant transitions for the proposed PNC experiment in a vapor cell.*

In a vapor cell experiment, it is desirable to employ buffer gas to limit diffusion of Yb atoms from the probe region. At sufficiently high buffer gas pressures, relatively large electric fields can be applied without breakdown, which is convenient for observing the Stark-induced $^1S_0 \rightarrow {}^3D_1$ transition. The optimal shot-noise-limited signal to noise ratio in a measurement of the $^3P_0$ population by absorption of 649 nm light is achieved with two absorption lengths at 649 nm [7]. If the $^3P_0$ quenching rate and pressure broadening of the 649 nm probe transition are sufficiently small, it is possible to build up a large population of absorbing atoms, allowing efficient detection of atoms having made the $^1S_0 \rightarrow {}^3D_1$ transition.

In the present experiment, quenching cross sections of the $^3P_0$ state and pressure broadening and shift of the 649 nm $^3P_0 \rightarrow {}^3S_1$ transition with respect to helium (He) and neon (Ne) are measured. The $^3P_0$ state is populated by exciting Yb atoms from the ground state to the 6s7p $^3P_1$ state with a pump laser light pulse (Fig. 2) followed by a cascade decay. The population of the $^3P_0$ state is continuously monitored by measuring absorption of probe laser light at 649 nm. The quenching rate is determined from the time dependence of the $^3P_0$ population. Measurements of the quenching rates at various buffer gas pressures and Yb densities yield upper limits on the $^3P_0$ quenching cross sections. The lineshape of the 649 nm transition in the vapor cell is obtained by measuring absorption as a function of probe beam frequency. In order to determine the pressure broadening and shift of the $^3P_0 \rightarrow {}^3S_1$ transition, the absorption profile is compared to a reference line observed by optogalvanic spectroscopy.

There have been a number of previous studies of depolarizing and elastic cross sections of the 6s6p $^3P_1$ (hereafter $^3P_1$) state [12-16], but the pressure broadening and shift

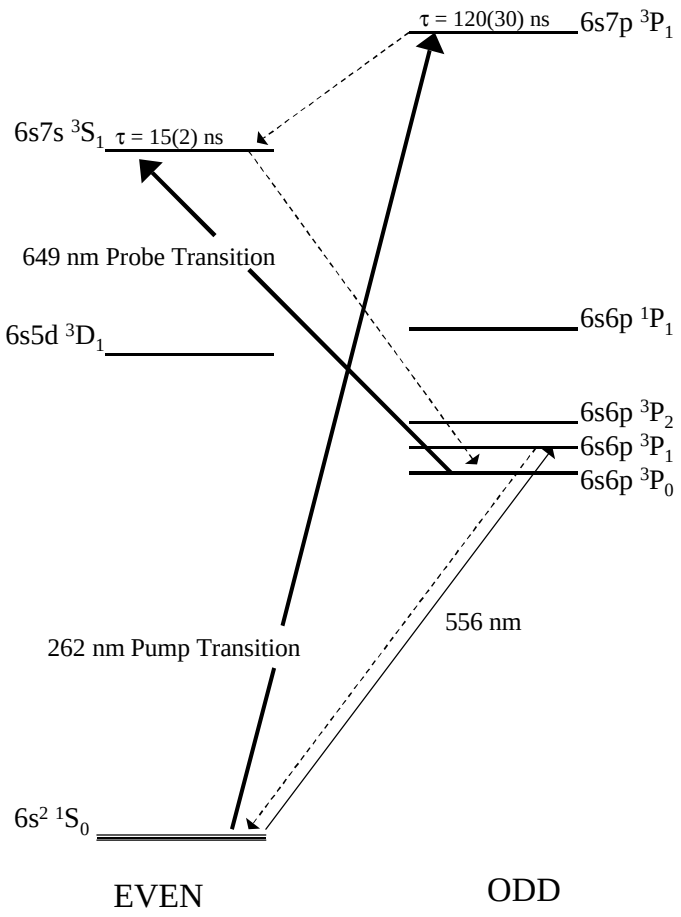

FIG. 2. *Partial energy level diagram of atomic ytterbium and relevant transitions for quenching cross section and pressure broadening and shift measurements. Lifetime of the 6s7s $^3S_1$ state is from [8-10], lifetime of the 6s7p $^3P_1$ state is from [11].*

of the 556 nm $^1S_0 \rightarrow {}^3P_1$ transition is measured here for the first time. Frequency calibration is performed by comparing absorption profiles in the vapor cell with fluorescence data from an Yb atomic beam.

In this paper, we first describe the experimental setup for measurement of quenching cross sections of the $^3P_0$ state and pressure broadening and shift of the 649 nm $^3P_0 \rightarrow {}^3S_1$ transition in Section 2.A. In Section 2.B. we describe the setup for measuring the pressure broadening and shift of the 556 nm $^1S_0 \rightarrow {}^3P_1$ transition. In Section 3 we

discuss the dependence of the absorption profile on various experimental parameters. The results are presented in Section 4. Finally, in Section 5 we consider the implications of these measurements for an ytterbium parity nonconservation experiment.

2. EXPERIMENTAL SETUP

A. $^3P_0$ Quenching Cross Sections and $^3P_0 \rightarrow {}^3S_1$ Pressure Broadening and Shift

The experimental apparatus for measuring the $^3P_0$ collisional quenching cross sections and 649 nm $^3P_0 \rightarrow {}^3S_1$ pressure broadening and shift is shown schematically in Fig. 3. A few grams of Yb (natural isotopic abundance) are placed in the center of a resistively heated, tantalum-lined stainless steel vapor cell. Before measurements are performed, the vapor cell is pumped down to ~ 10^{-2} Torr with a mechanical vacuum pump and baked overnight at 500 K to remove impurities. In order to reduce the introduction of impurities into the cell, gas lines in and out of the vapor cell pass through a liquid nitrogen trap. A trap filled with steel wool is in line between the mechanical pump and the vapor cell to prevent cell contamination with vacuum pump oil.

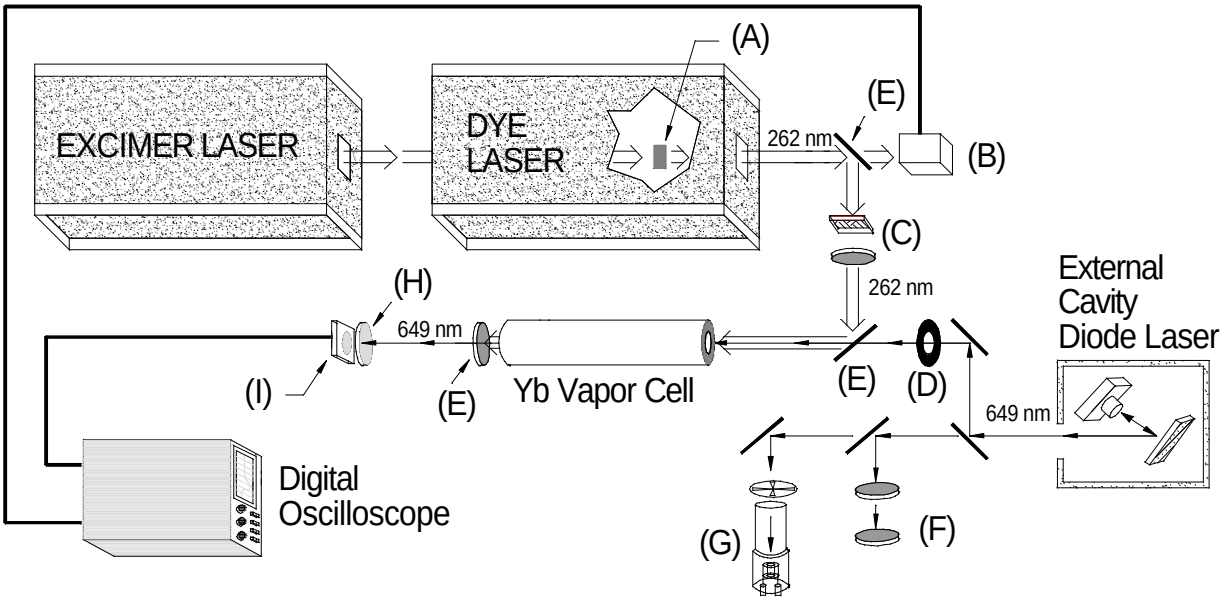

FIG. 3. *Experimental setup for Yb 6s6p $^3P_0$ collisional de-excitation cross section and 649 nm 6s6p $^3P_0$ ® 6s7s $^3S_1$ pressure broadening and shift measurements: (A) BBO crystal; (B) Fast photodiode trigger; (C) UV filter and lens to expand 262 nm beam diameter; (D) Iris; (E) Dichroic mirror; (F) confocal scanning Fabry-Perot; (G) Yb hollow cathode lamp; (H) 650 nm interference filter; (I) photodiode.*

Cross section and pressure broadening and shift measurements were performed at a temperature of 700 ± 10 K in the central region of the vapor cell (the middle 20 cm heated by a ceramic beaded heater [17]). The temperature of the central region measured with a thermocouple is consistent with that deduced from the observed Doppler width of Yb resonance lines. For some data sets, the Yb density is monitored by observing the absorption of 556 nm light tuned near the $^1S_0 \rightarrow {}^3P_1$ transition. The Yb density is in agreement with the predicted saturated vapor pressure [18], corresponding to an average Yb density of ~ 5×10^{12} atoms/cm^3 in the central region. The column length of ytterbium vapor is approximately 20 cm, roughly matching the length of the heated central region of the vapor cell. Buffer gas pressure in the vapor cell is monitored by two capacitance manometers (MKS Baratrons) with ranges of 100 Torr and 5000 Torr.

The pulsed 262 nm pump beam is produced by an excimer (Lambda Physik EMG 101 MSC) pumped dye laser (Lambda Physik FL 2002) with frequency doubling. Coumarin 521 dye generates light at 524 nm. The 524 nm light passes through a BBO crystal to produce second harmonic light at 262 nm. The laser system operates with a repetition rate of 5 Hz and each pulse at 262 nm has an energy of ≈ 0.5 mJ, a duration of ≈ 20 ns and a spectral width of ≈ 0.5 cm^{-1}. A lens expands the 262 nm beam diameter to ≈ 1 cm in the central interaction region of the vapor cell. The 262 nm pump beam has a broad spectral width, so all isotopic and hyperfine components of the 6s7p $^3P_1$ state, and consequently the $^3P_0$ state, are populated. The pump beam spectral width is larger than the Doppler width, so velocity changing collisions do not affect the probe signal. The pump beam typically transfers 5-10% of the ground state population to the $^3P_0$ state.

The 649 nm probe beam is generated by a home-made external cavity diode laser system [19]. The single frequency output is typically 10 mW, tunable over approximately 3-5 GHz without mode hops or multimode behavior. The spectrum of the diode laser is monitored with a confocal scanning Fabry-Perot interferometer.

Most of the probe laser output is directed into a commercial Yb hollow cathode lamp [20] filled with neon buffer gas. We use the optogalvanic signal from the hollow cathode lamp to tune the probe laser to resonance with the $^3P_0 \rightarrow {}^3S_1$ transition [7]. The spectrum of the $^3P_0 \rightarrow {}^3S_1$ transition measured with optogalvanic spectroscopy is shown in Fig. 4.

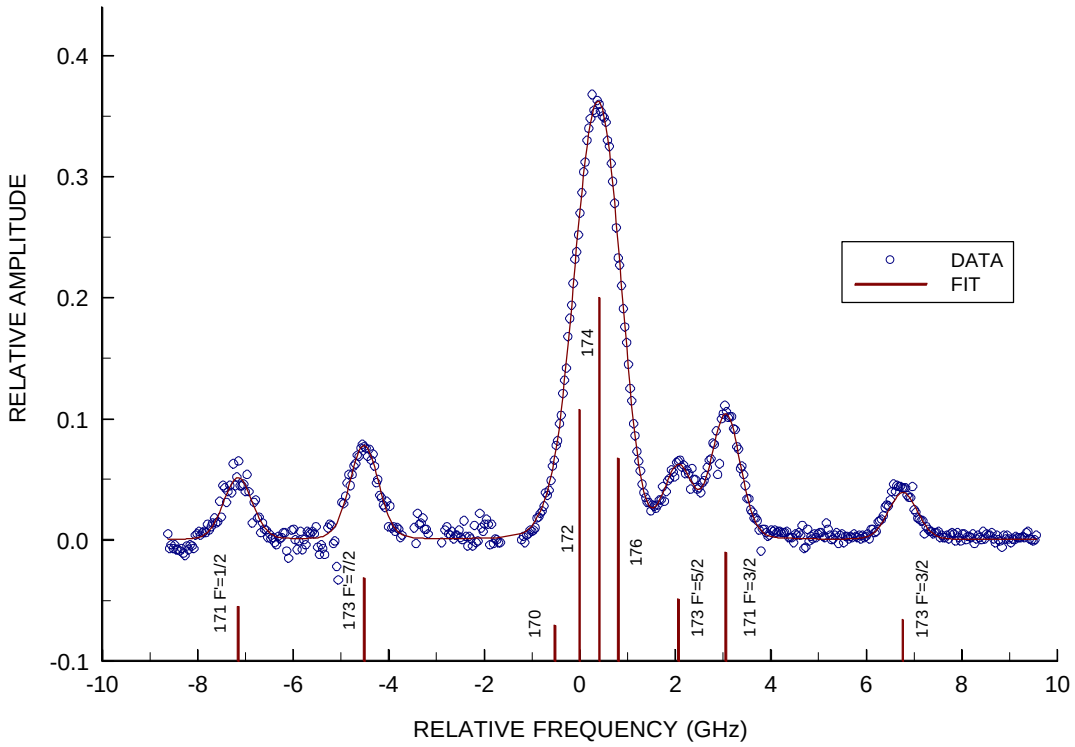

FIG. 4. *Optogalvanic spectrum of the 649 nm $^3P_0$ ® $^3S_1$ transition. Our results for the isotope shifts and hyperfine structure agree with previous measurements [21-23]. Isotopic components are labeled with the respective atomic masses and F' is the total angular momentum of the upper state of a hyperfine transition.*

The probe beam diameter is reduced to ≈ 1 mm before entering the vapor cell and its power is attenuated to < 1 μW. We find that at this laser intensity the probe beam does not significantly affect the population of the metastable $^3P_0$ state compared to other loss mechanisms, in agreement with estimates of optical pumping rates [7].

The probe and pump beams are aligned collinearly on the axis of the vapor cell, with the smaller probe beam centered inside the larger pump beam. This geometry ensures that at sufficient buffer gas pressures, atoms in the metastable $^3P_0$ state diffuse out of the pump region more slowly than they are quenched by collisions (i.e. the quenching rate significantly exceeds the diffusion rate $\Gamma_{quench} >> \Gamma_D$). We verify experimentally that slight misalignment of the beams has no discernible effect on measurements.

The 262 nm beam is retro-reflected by a dichroic mirror as it exits the cell, while the 649 nm light is transmitted. The probe beam intensity after passing through the cell is measured with a photodiode fitted with a 650 nm central wavelength interference filter with a 10 nm bandwith.

B. Pressure Broadening and Shift of the $^1S_0 \rightarrow {}^3P_1$ Transition

The pressure broadening and shift of the 556 nm $^1S_0 \rightarrow {}^3P_1$ transition is determined by comparing the absorption spectrum in the vapor cell to fluorescence from an Yb atomic beam. Light at 556 nm is generated by a ring dye laser (Spectra-Physics 380D, using Rhodamine 110) pumped by an Ar^+ laser (for these measurements, the pulsed 262 nm pump beam is absent). The atomic beam apparatus is essentially the same as that used in our previous work, described in detail in [4]. Light at 556 nm excites

atoms in the atomic beam to the $^3P_1$ state and fluorescence at 556 nm is detected with a photomultiplier tube. A portion of the laser output is coupled into a single-mode optical fiber which takes the light into a different laboratory where measurements with the vapor cell are performed. Photodiodes monitor the intensity of incident light before and after passing through the cell. The power of the light passing through the vapor cell is attenuated to less than 500 nW, far below saturation of the transition. The laser is scanned over 20 GHz for lineshape measurements. For high Yb densities and buffer gas pressures – when the lines in the vapor cell are broad – it is necessary to concatenate multiple scans to determine both the shape of the wings and the position of the line center. Frequency markers from Fabry-Perot interferometers and isotope shifts and hyperfine structure of the $^1S_0 \rightarrow {}^3P_1$ transition allow us independent ways to calibrate the frequency scans of the laser.

3. DEPENDENCE OF THE ABSORPTION PROFILE ON EXPERIMENTAL PARAMETERS

The intensity of light $I(w,t)$ transmitted through the ytterbium vapor cell is described by:

$$I(w,t) = I_0(w)e^{-a(w,t)l}, \tag{1}$$

where $I_0(w)$ is the light intensity before entering the vapor cell, l is the column length of the Yb vapor and $a(w,t)$ is the absorption coefficient, given by:

$$a(w,t) = \frac{3pc^2 n(t)}{w_0{}^3 t}\frac{w}{g_D}V(w) = a(w,0)\frac{n(t)}{n(0)}, \tag{2}$$

where $n(t)$ is the density of Yb atoms in the lower state of a given transition within the probe region at time t, w_0 is the resonant frequency of the transition, w is the frequency of the probe laser, t is the upper state lifetime (t = 15(2) ns for the $^3S_1$ state [8-10] and t = 872(2) ns for the $^3P_1$ state [24]), g_D is the Doppler width and $V(w)$ is the Voigt lineshape function ($V(w)$ includes relative intensities of hyperfine components and isotopic abundance). Self-broadening (which could mimic a change in $^3P_0$ population by causing $V(w)$ to acquire a time dependence) was found to be insignificant [7]. Thus, a measurement of the intensity of light transmitted through the vapor cell directly determines the density of Yb atoms in the $^3P_0$ state as a function of time.

Yb atoms in the $^3P_0$ state are lost from the probe region by diffusion and quenching by buffer gas atoms, Yb atoms (both in the ground state and excited states), and possible gaseous impurities. Measurements of $^3P_0$ loss rates with respect to 262 nm pump beam power and Yb density indicate that quenching cross sections for ground state and excited state Yb atoms are roughly the same ($s_{Yb} \sim 10^{-14}$ cm^2) [7]. Branching ratio estimates indicate that ~ 70-80% of Yb atoms are in the ground state ~ 200 ns after excitation by the 262 nm pump pulse. Therefore we assume Yb-Yb quenching is primarily due to atoms in the ground state, and include contributions from excited state quenching in our uncertainties.

The diffusion rate of Yb atoms in the $^3P_0$ state from the probe region decreases as buffer gas density is increased, while collisional quenching rates increase with perturber density. Therefore, it is straightforward to distinguish collisional quenching from any losses due to diffusion. Data are taken at sufficiently high buffer gas pressure ($\geq$ 100 Torr) where losses by diffusion are negligible.

Since we operate in the regime of low buffer gas density ($s^{1/2} < n^{-1/3}$), we consider only two-body collisions in the impact approximation [25]. The time dependence of the population of the 6s6p $^3P_0$ state is given by:

$$\frac{dn}{dt} \cong -\Gamma n \cong -\left(\Gamma_B + \Gamma_{Yb} + \Gamma_I\right)n\,, \tag{3}$$

where n is the density of Yb atoms in the $^3P_0$ state, Γ is the total $^3P_0$ Yb loss rate from the probe region, and Γ_B, Γ_{Yb} and Γ_I are the quenching rates due to collisions with buffer gas atoms, ground state Yb atoms and residual gaseous impurities respectively. Therefore

$$n(t) = n(0)e^{-\Gamma t}\,, \tag{4}$$

where $n(0) \approx 10^{11}$ cm^{-3} is the initial density of Yb atoms in the $^3P_0$ state just after excitation by the 262 nm pump pulse. Under typical experimental conditions, the sum of the quenching rates due to Yb atoms and/or possible gaseous impurities is ~ 300-500 s^{-1} as determined from loss rates extrapolated to zero buffer gas pressure. The quenching rate with respect to the buffer gas Γ_B depends linearly on the buffer gas density n_B:

$$\Gamma_B = n_B \cdot s_B \cdot \bar{v}_{rel}\,, \tag{5}$$

where s_B is the quenching cross section for this process and

$$\bar{v}_{rel} = \left(\frac{8k_B T}{pm}\right)^{1/2} \tag{6}$$

is the average relative velocity between colliding Yb atoms and buffer gas atoms, m is the reduced mass of the Yb-buffer gas atom system, k_B is Boltzmann's constant and T is the temperature. If ytterbium and impurity densities in the vapor cell are independent of buffer gas pressure, so are Γ_{Yb} and Γ_I .

The normalized Voigt lineshape function $V(w)$ in equation (2) is given by [26]:

$$V(w) = \sum_j C_j g\left(z_j(w)\right), \tag{7}$$

where the index *j* refers to various isotopic and hyperfine components, the C_j's are constants which account for the isotopic abundance and relative intensity of particular hyperfine components and

$$g\left(z_j(w)\right) = \mathrm{Re}\left(\sqrt{p}\cdot\exp\left[-z_j(w)^2\right]\cdot\left(1-\Phi\left[-iz_j(w)\right]\right)\right). \tag{8}$$

Here $\Phi[x]$ is the complex error function [27] and

$$z_j(w) = \frac{w - w_j}{g_D} + i\left(\frac{g_N + g_P}{2g_D}\right), \tag{9}$$

where w_j is the resonance frequency of a particular isotopic or hyperfine component, g_N is the natural width and g_P is the pressure width. Determination of the absorption coefficient as a function of probe laser detuning allows us to extract both the Doppler and pressure widths. We use previously measured values for the separation of hyperfine and isotope components in our fits [21-23, 28-30]. We assume the same broadening and shift for all hyperfine components.

4. RESULTS AND DISCUSSION

A. $^3P_0$ Quenching Cross Sections

Yb atoms excited from the ground state to the 6s7p $^3P_1$ state by the 262 nm pump beam populate the $^3P_0$ state via cascade decay within about 150 ns. Once the $^3P_0$ state is populated, the medium is no longer transparent to the 649 nm probe beam (equations (1) and (2)). The photodiode detector circuit which monitors probe beam intensity after passing through the cell has a finite response time $t_r \approx 50$ μsec. At times *t* much longer

than t_r the voltage signal $j(t)$ from the photodiode is given by an approximation to a convolution of the detector response function with the input signal [7]:

$$j(t) = A_0 \exp[-a(w,0)l \exp[-\Gamma t]], \tag{10}$$

where A_0 is an amplitude factor proportional to incident light intensity. For each pulse the experimental signal is saved to computer and fit to equation (10). Analysis yields values for the total loss rate Γ and the absorption coefficient $a(w,0)$. A typical fit is shown in Fig. 5.

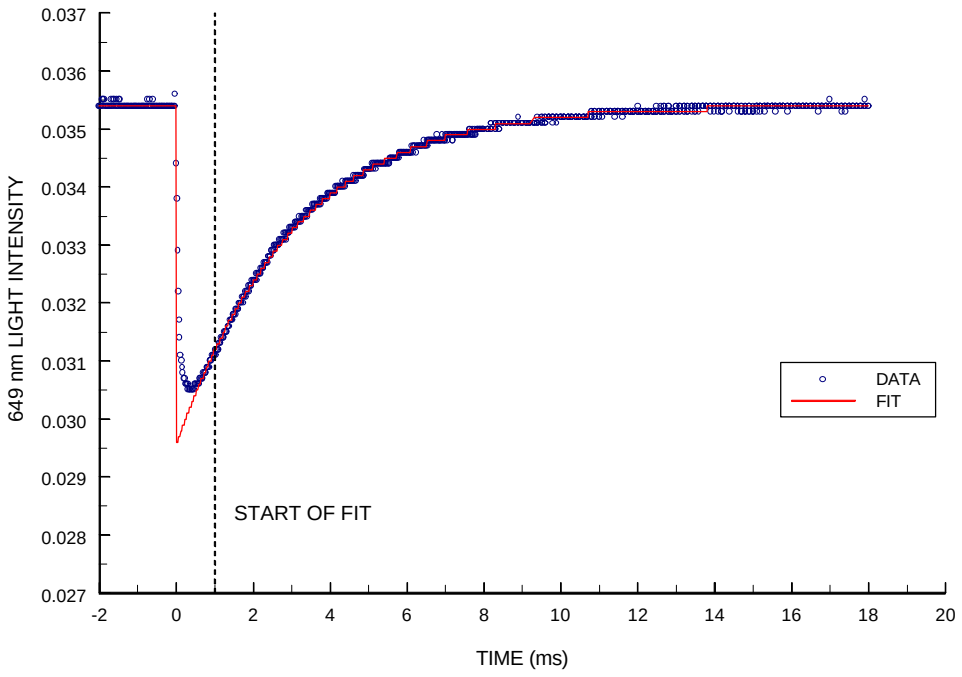

FIG. 5. *Intensity of 649 nm light transmitted through the vapor cell. This particular data set is with neon buffer gas at a pressure of 100 Torr. The 262 nm pulse passes through the vapor cell at t = 0, populating the 6s6p $^3P_0$ state. The fit is performed with data after t = 1 ms where the photodiode circuit response effects have died away.*

Data are taken at buffer gas pressures ranging from 100 to 600 Torr. At higher pressures, collisional broadening of the probe transition reduces the signal to noise ratio

to less than one. Below approximately 100 Torr, diffusion dominates over quenching. Fig. 6 shows the total loss rate Γ with respect to He and Ne densities.

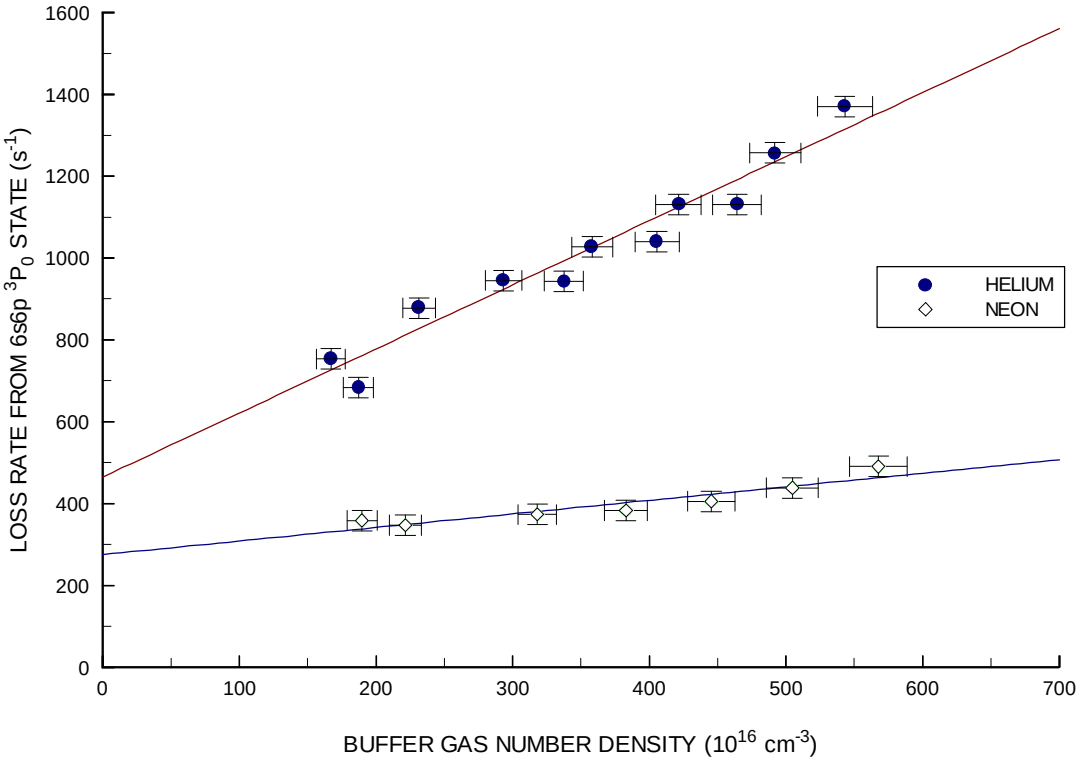

FIG. 6. *Total loss rate G of Yb atoms in the 6s6p $^3P_0$ state from the probe region with respect to buffer gas density. Each data point is the average of 4-8 laser pulses. The straight lines are least squares fits. The difference between the y-intercepts of the two data sets is consistent with changes in $^3P_0$ loss rates due to variations in ytterbium density between runs.*

The quenching cross sections with respect to He and Ne are small ($s_B \lesssim 10^{-21}$ cm^2). Therefore, although our observations are consistent with quenching by buffer gas atoms, it is possible that a slight dependence of Yb or impurity density on buffer gas pressure could account for the linear dependence of Γ on buffer gas density seen in Fig.6. For this reason, we interpret our results as an upper limit for the $^3P_0$ quenching rate due to collisions with buffer gas atoms (equation (5)). Sources of uncertainty in the

measurements of quenching rates at different buffer gas pressures and their contribution to the uncertainty in s_B are summarized in Table I, briefly explained below and considered in more detail in [7].

Table I. – Sources of uncertainty in determination of s_B in units of 10^{-22} cm^2.

SOURCE OF UNCERTAINTY	HELIUM	NEON
Variation of Yb density	1.0	1.9
Quenching by excited state Yb	2.5	2.5
Uncertainty in buffer gas density	0.7	0.3
Change in Γ with start time of fit	4.1	1.2
Statistical	0.5	0.4
TOTAL	5.0	3.5

Measurement of Yb density variations with respect to buffer gas pressure at fixed cell temperature provides a limit on the uncertainty in s_B from quenching by Yb atoms, $d(s_B)_{Yb}$:

$$d(s_B)_{Yb} \le \frac{\Delta n_{Yb}}{\Delta n_B} \frac{\bar{v}_{rel}(Yb-Yb)}{\bar{v}_{rel}(Yb-B)} s_{Yb}, \qquad (11)$$

where Δn_{Yb} is the upper limit on change in Yb density for a given change in buffer gas density Δn_B. Although the measurements for He and Ne were performed near the same vapor cell temperature (700 K), the total Yb density probably differed between runs. A relatively small difference in cell temperature between runs (10 K) leads to a substantial difference in Yb density (30%) [18]. This may account for the difference between extrapolated quenching rates at zero buffer gas pressure for He and Ne in Fig. 6 (Yb density was not monitored directly in these experimental runs).

Quenching by excited state Yb atoms also introduces a systematic uncertainty. As buffer gas density changes, relative populations of ground and excited state Yb atoms may change. The contribution of this uncertainty to s_B is constrained by Yb density measurements and estimates of excited state quenching cross sections [7].

Since the cell is pumped down to 10^{-2} Torr, it is possible that the impurity density in the cell could be as large as 10^{14} cm^{-3}. In principle, impurity density may be proportional to buffer gas density, so gaseous impurities in the cell can add to the measured value of s_B.

Buffer gas density was deduced from the measured pressure and temperature in the interaction region. Hence, uncertainties in buffer gas pressure and cell temperature lead to an uncertainty in buffer gas density.

An additional systematic uncertainty arises from a slight dependence of the deduced value of Γ on the start time of the fit, indicating that equation (10) is not a perfect description of our data. This discrepancy may be attributed to quenching by Yb atoms in excited states or a non-uniform Yb density distribution within the probe region [7]. These effects can lead to a more complicated time dependence of the transmitted light intensity than assumed in equation (10). The change in the quenching rate with the start of the fit is relatively small (~5%), so we include it as an uncertainty in the cross section values.

Considering these uncertainties, we find that $s_{He} < 13 \times 10^{-22}$ cm^2 and $s_{Ne} < 8 \times 10^{-22}$ cm^2.

B. Pressure Broadening and Shift of the $^3P_0 \rightarrow {}^3S_1$ Transition

Varying the frequency of the 649 nm probe light allows us to determine the lineshape of the $^3P_0 \rightarrow {}^3S_1$ transition at various buffer gas pressures. The intensity of 649 nm light transmitted through the vapor cell is measured at a fixed time after the pump pulse populates the $^3P_0$ state. We fit the data to equation (1) using the frequency dependent absorption coefficient (equation (2)) and extract the pressure width from the normalized Voigt profile (equations (7-9)). Comparison with the simultaneously recorded optogalvanic signal from the Yb hollow cathode lamp allows us to determine the relative pressure shift. Typical data is shown in Fig. 7. The Doppler width is

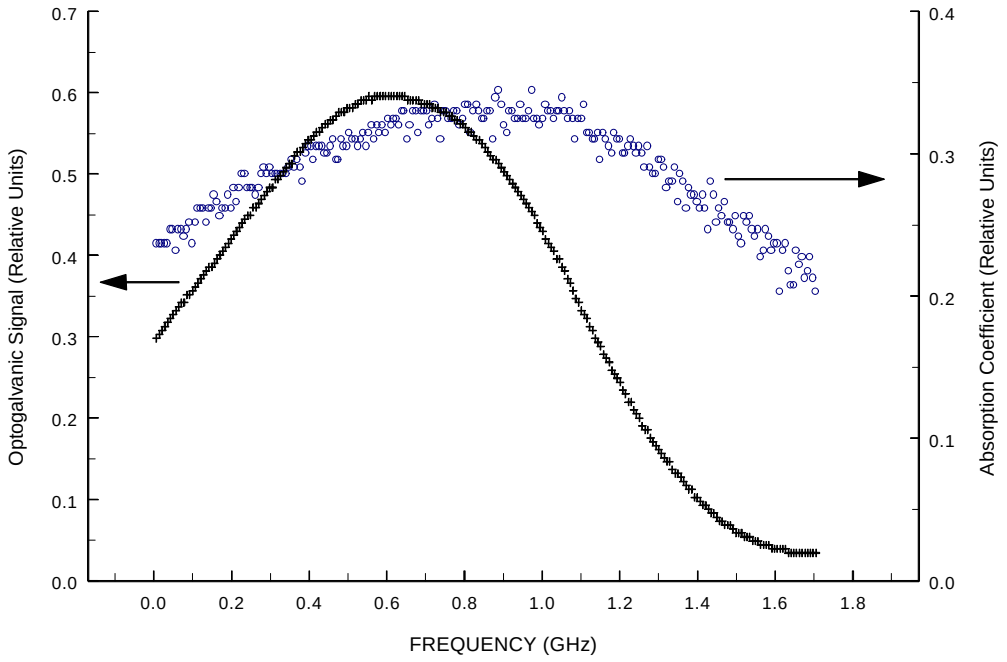

FIG. 7. *Typical data for measurement of pressure broadening and shift of the 649 nm 6s6p $^3P_0$ ® 6s7s $^3S_1$ transition. This data set focuses on the even isotope components (see Fig. 4) at a helium pressure of 70 Torr.*

determined by fits to data near zero buffer gas pressure, and is in agreement with the observed temperature in the central region of the vapor cell. Fits to a Voigt profile with the Doppler width held constant determine the width due to collisional broadening. Pressure shift and width at various He and Ne pressures are plotted in Fig. 8, and the

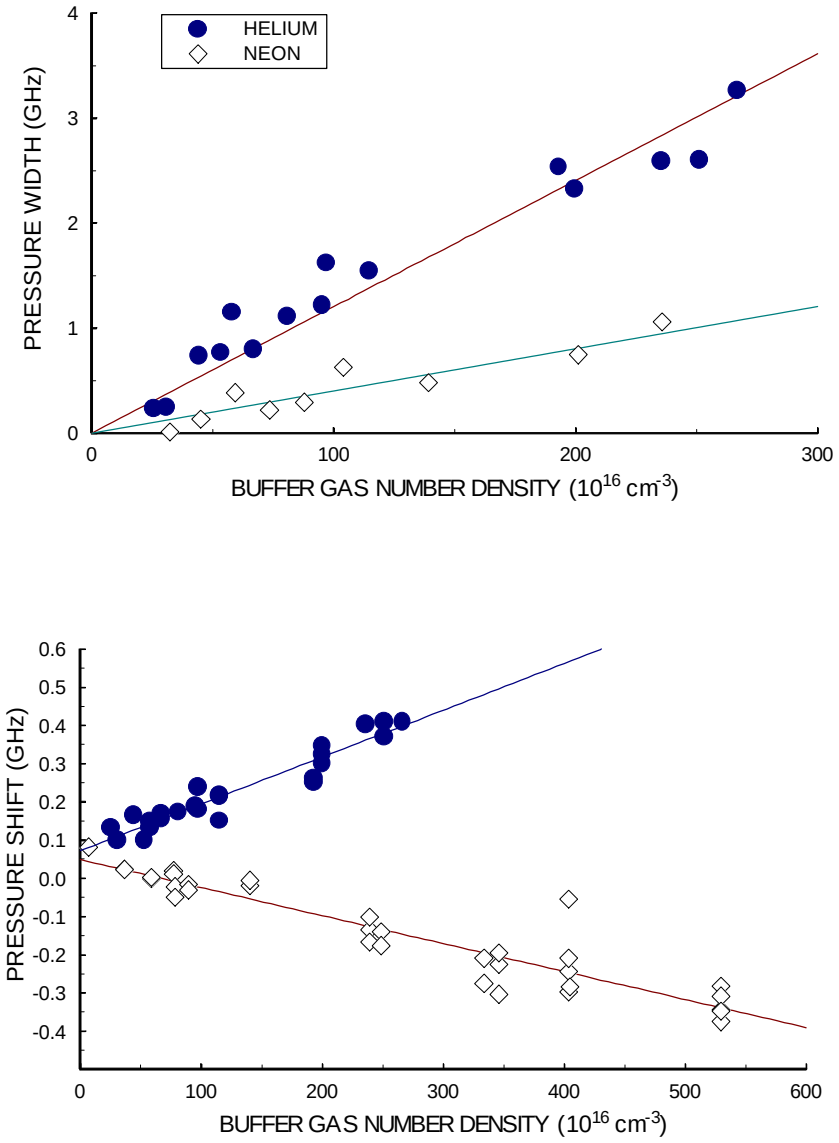

FIG. 8. *Pressure broadening and shift of the 649 nm 6s6p $^3P_0$ ® 6s7s $^3S_1$ transition by helium and neon.*

results for the pressure broadening and shift of the $^3P_0 \rightarrow {}^3S_1$ transition are given in Table II. Systematic uncertainties due to laser frequency scan nonlinearity and uncertainties in the vapor cell temperature and buffer gas pressure were found to be on the order of the statistical spread of the points. Possible gaseous impurities in the cell do not significantly affect these measurements since buffer gas induced broadening and shift cross sections are of the usual size (10^{-15} to 10^{-14} cm^2) and the impurity density is relatively low.

Table II. – Pressure Broadening and Shift rates (Γ / n) in units of 10^{-9}s^{-1}cm^3.

	HELIUM		**NEON**	
Transition	Broadening	Shift	Broadening	Shift
649 nm 6s6p $^3P_0 \rightarrow$ 6s7s $^3S_1$	7.5 ± 1.3	0.8 ± 0.1	2.5 ± 0.3	-0.5 ± 0.1
556 nm 6s^2 $^1S_0 \rightarrow$ 6s6p $^3P_1$	3.8 ± 0.1	0.0 ± 0.5	1.5 ± 0.1	-0.5 ± 1.0

C. Pressure Broadening and Shift of the $^1S_0 \rightarrow {}^3P_1$ Transition

The intensity of 556 nm light transmitted through the vapor cell is also described by equation (1), but in this case the absorption coefficient is time independent. Pressure broadening of the $^1S_0 \rightarrow {}^3P_1$ transition is found from fits to the 556 nm absorption profile (equations (1-2) and (7-9)). The pressure shift is determined by comparing the 556 nm fluorescence from the atomic beam to absorption in the vapor cell (Fig. 9). Fig. 10 shows a plot of the pressure broadening as a function of He and Ne number densities. The results are presented in Table II. The scatter of shift data is relatively large due to the difficulty in absolute frequency calibration of the featureless absorption profile at high buffer gas density. Least squares fits give shifts consistent with zero for both He and Ne.

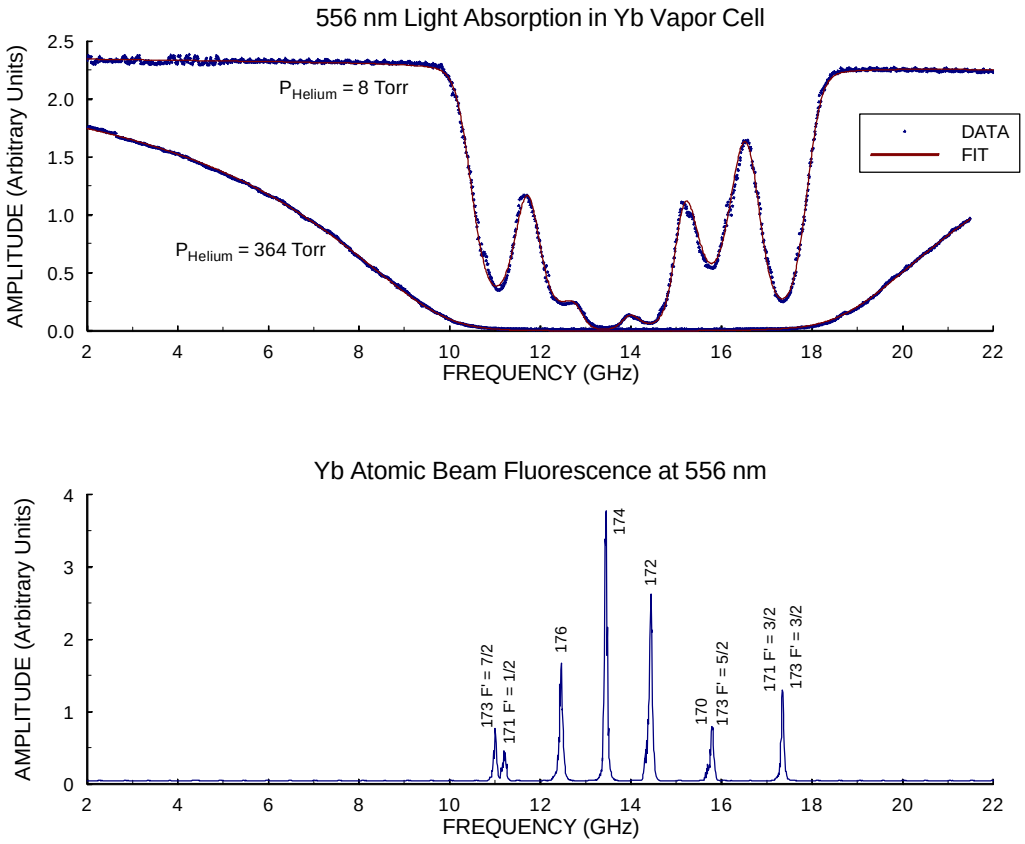

FIG. 9. *Typical data for measurement of the pressure broadening and shift of the 556 nm $6s^2\ ^1S_0$ ® $6s6p\ ^3P_1$ transition. For atomic beam fluorescence data, isotopic components are labeled with the respective atomic masses and F' is the total angular momentum of the upper state of a hyperfine transition.*

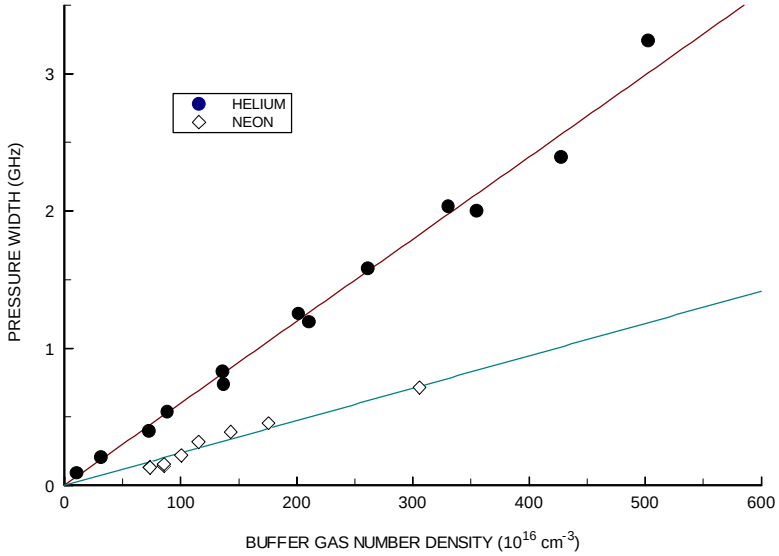

FIG. 10*. Pressure broadening of the 556 nm $6s^2\ ^1S_0$ ® $6s6p\ ^3P_1$ transition.*

5. CONSEQUENCES FOR A PARITY NONCONSERVATION EXPERIMENT

The exceptionally small collisional de-excitation cross sections of the $^3P_0$ state may make an Yb PNC experiment in a vapor cell advantageous. A possible configuration for such an experiment is shown in Fig. 11. Here the PNC observable is a difference in transition rates arising from the interference of Stark-induced and PNC-induced transition amplitudes for right- and left-handed experimental configurations. This geometry is similar to that of the PNC experiment performed with cesium by the group in Boulder [31]. The asymmetry corresponding to the pseudoscalar rotational invariant $\vec{s}\cdot\left(\vec{E}\times\vec{B}\right)$ would be measured by comparing how many Yb atoms are excited to the upper state of the 408 nm $^1S_0 \rightarrow {}^3D_1$ transition for different orientations of $\vec{s}$ (angular momentum of excitation photons), $\vec{E}$ (static electric field), and $\vec{B}$ (static magnetic field).

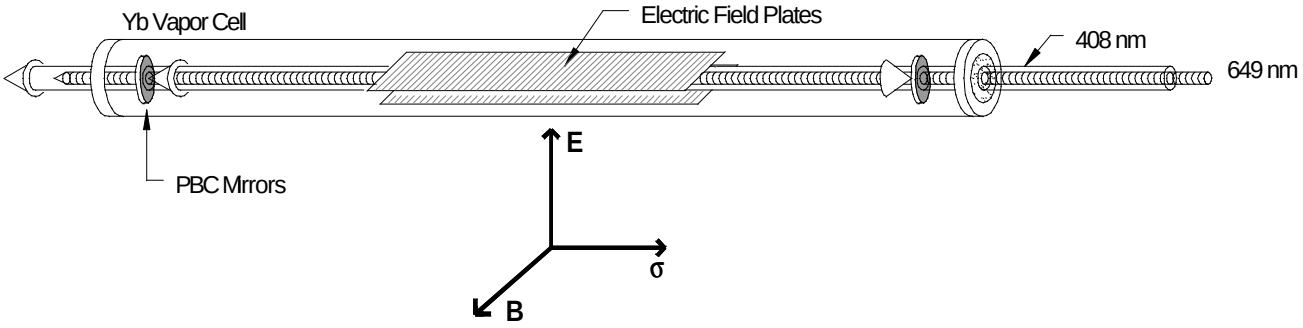

FIG. 11. *Schematic diagram of the apparatus for a proposed Yb PNC experiment in a vapor cell.*

In an envisioned PNC experiment, Yb atoms will be excited to the $^3D_1$ state by 408 nm light produced by directing continuous wave laser light into a multipass cavity or a power buildup cavity. Most of the atoms excited to the $^3D_1$ state subsequently decay to the $^3P_0$ state. As in the present work, the $^3P_0$ population will be monitored with a weak probe beam at 649 nm (Fig. 1). Performing a parity violation measurement in a vapor

cell offers a number of potential advantages compared to a similar experiment in an atomic beam. A vapor cell enables higher counting rates due to greater atomic density and volume in the probe region, and greater detection efficiency is achieved by measuring absorption of a probe laser as opposed to measuring fluorescence. Optimization of the experimental conditions for a PNC experiment in a cell will depend on parameters which are not currently known (e.g., the $^1S_0 \rightarrow {}^3D_1$ pressure broadening). Here, we point out that with plausible conditions (similar to those used in this work where possible), a vapor cell PNC experiment with Yb indeed appears to give improved sensitivity compared to a beam experiment.

We conservatively estimate that the cavity inside the vapor cell should be able to achieve a gain of 500 (about 2 orders of magnitude less than that achieved by the Boulder group [31], due to the use of a vapor cell rather than an atomic beam). With an input power of ≈ 200 mW, this is sufficient to produce approximately 100 W of power at 408 nm in the interaction region. Two absorption lengths at the probe transition requires a density of ~ 10^{10} Yb atoms per cm^3 in the $^3P_0$ state (for a 50 cm long interaction region). After pumping for a sufficiently long time ($> \Gamma_{pump}^{-1}$):

$$n_{3P0} = \frac{\Gamma_{pump}}{\Gamma_{loss}} n_{total}, \tag{17}$$

where the pumping rate Γ_{pump} (in s^{-1}, assuming a beam diameter of ≈ 1mm) is given by:

$$\Gamma_{pump} \approx \frac{\left(|b| E_{stat} E_{408}\right)^2}{g_R}, \tag{18}$$

where E_{stat} is the static electric field, E_{408} is the electric field amplitude of the 408 nm light, and γ_R is the larger of either the Doppler or pressure widths (depending on cell

conditions). For example, using neon as the buffer gas at a pressure of ≈ 400 Torr and at a cell temperature of ≈ 700 K (yielding a total Yb density of 5×10^{12} atoms/cm^3), the necessary static electric field is ≈ 900 V/cm. For an electric field plate separation of 1 cm the breakdown voltage for neon under these conditions is ≈ 1750 V/cm [32], so such a field amplitude is probably achievable in the proposed experimental configuration.

The fractional uncertainty in a measurement of $E1_{PNC}$ can be estimated to be:

$$\left(\frac{dE1_{PNC}}{E1_{PNC}}\right)^2 \approx \frac{N_{total}}{\left(\Delta N_{PNC}\right)^2}, \tag{19}$$

where N_{total} is the total number of atoms detected in the $^3P_0$ state:

$$N_{total} \approx \frac{\left(|b|E_{stat}E_{408}\right)^2}{g_R} N_{Yb} T e_d \tag{20}$$

and ΔN_{PNC} is the difference in the total number of atoms detected in the $^3P_0$ state between different $\vec{E}_{stat}$ orientations (the asymmetry due to PNC-Stark interference), given by:

$$\Delta N_{PNC} \approx \frac{4|b|E_{stat}E1_{PNC}E_{408}^2}{g_R} N_{Yb} T e_d, \tag{21}$$

where $E1_{PNC}$ is the PNC-induced $E1$ amplitude for the 408 nm transition, N_{Yb} is the total number of Yb atoms in the interaction region, T is the measurement time in seconds and e_d is the detection efficiency. This yields an uncertainty in $E1_{PNC}$ of

$$\left(dE1_{PNC}\right)^2 \approx \frac{1}{T}\left(\frac{g_R}{16E_{408}^2 N_{Yb} e_d}\right). \tag{22}$$

As is commonly the case in Stark-PNC interference experiments, there is no dependence on the static electric field [33].

Table III. – Estimated experimental parameters for Yb PNC experiment in a vapor cell and an atomic beam.

Parameter	***Cell***	***Beam***
E_{408}	3 kV/cm	12 kV/cm
γ_R	$2\pi\cdot$1000 MHz (Pressure width)	$2\pi\cdot$30 MHz (Doppler Width)
ε_d	1	0.1
N_{Yb}	2.5×10^{11} atoms	2×10^{8} atoms

We can now compare the statistical sensitivity of such an Yb PNC experiment performed in a vapor cell to a similar experiment in an Yb atomic beam. Based on estimates of experimental parameters from this work for a vapor cell and [1,4,5] for an atomic beam (presented in Table III), we find from equation (22) the fractional uncertainties in $E1_{PNC}$ for a cell experiment and a beam experiment to be:

$$\left(\frac{dE1_{PNC}}{E1_{PNC}}\right)^2_{cell} \approx \frac{5\times10^{-6}}{T}$$

$$\left(\frac{dE1_{PNC}}{E1_{PNC}}\right)^2_{beam} \approx \frac{10^{-4}}{T}.$$

This demonstrates that an Yb vapor cell experiment may offer advantages in statistical sensitivity to PNC effects in comparison to an atomic beam experiment.

However, there remain a number of issues that need to be addressed before pursuing an Yb PNC experiment in a vapor cell. These include collisional broadening of the 408 nm $^1S_0 \rightarrow {}^3D_1$ transition, ionization of Yb atoms by the 408 nm light, and collisionally assisted transition rates to the $^3D_1$ state. These questions will be addressed in future experimental work.

6. CONCLUSION

We have placed upper limits on the collisional quenching cross sections of the 6s6p $^3P_0$ metastable state in atomic ytterbium with respect to helium and neon. The cross sections are sufficiently small so that quenching is not a limiting factor for the proposed Yb PNC cell experiment. In addition we have measured the pressure broadening and shift of the 6s6p $^3P_0 \rightarrow$ 6s7s $^3S_1$ and 6s^2 $^1S_0 \rightarrow$ 6s6p $^3P_1$ transitions. Future work will involve the construction of a new vapor cell with electric field plates. This new apparatus will allow us to further investigate the feasibility of an Yb PNC experiment in a vapor cell. In order to obtain values for the quenching cross sections of the 6s6p $^3P_0$ metastable state improved vacuum, gas handling, and heating systems will be employed. This will further eliminate gaseous impurities and allow better control of Yb density.

ACKNOWLEDGMENTS

The authors wish to thank C.J. Bowers, D.E. Brown, E.D. Commins, B. DeBoo, A.-T. Nguyen, and V.V. Yashchuk for useful discussions and assistance during the experiments, R.W. Falcone for providing the excimer laser and his continued interest in this work, and M. Solarz and A. Vaynberg for help in construction of the apparatus. Important contributions to early stages of the project were made by M. Lintz, made possible by the France-Berkeley fund. One of us (D.F.K.) was a Berkeley Physics Undergraduate Research Scholar and the recipient of a University of California at Berkeley Undergraduate Research Apprentice summer stipend. This work has been supported by UC Berkeley Committee on Research and the LBNL Nuclear Science Division under U.S. Department of Energy Contract No. DE-AC03-76SF00098.

---

[1] D. DeMille, Phys. Rev. Lett. **74**, 4165 (1995).

[2] S.G. Porsev, Yu.G. Rakhlina, and M.G. Kozlov, Pis'ma Zh. Eskp. Teor. Fiz. **61**, 449 (1995); JETP Lett. **61** 459 (1995).

[3] B.P. Das, *Phys. Rev. A* **56**, 1635 (1997).

[4] C.J. Bowers, D. Budker, D. DeMille, S.J. Freedman, G.Gwinner, and J.E.Stalnaker, APS e-print #aps1999jan03_001; C.J. Bowers, Ph.D. thesis, University of California at Berkeley (1998). Available in electronic form at http://phylabs.berkeley.edu/bowers.

[5] J.E. Stalnaker, Undergraduate Thesis, University of California at Berkeley (1998). Available in electronic form at http://phylabs.berkeley.edu/budker.

[6] An experiment to precisely measure this branching ratio (to a few %) is currently in progress in this laboratory.

[7] D.F. Kimball, Undergraduate Thesis, University of California at Berkeley (1998). Available in electronic form at http://phylabs.berkeley.edu/budker.

[8] M. Baumann, M. Braun, A. Gaiser, and H. Liening, J. Phys. B. **18**, L601 (1985).

[9] W. Lange, J. Luther, and A. Steudel, *Proc. 2nd EGAS Conf.* (1970) (unpublished).

[10] C.H. Corliss and W.R. Bozman, *NBS Monograph* No. 53 (Washington, DC: US Govt. Printing Office) p.532 (1962).

[11] C.J. Bowers, D. Budker, E.D. Commins, D. DeMille, S.J. Freedman, A.-T. Nguyen, S.-Q. Shang, and M. Zolotorev, Phys. Rev. A **53**, 3103 (1996).

[12] F.H.K. Rambow and L.D. Schearer, Phys. Rev. A **14**, 738 (1976).

[13] J.-C. Keller and J.-L. Le Gouet, Phys. Rev. Lett. **52**, 2034 (1984); Phys. Rev. A **32**, 1624 (1985).

[14] A.P. Ghosh, C.D. Nabors, M.A. Attili and J.E. Thomas, Phys. Rev. Lett. **54**, 1794 (1985).

[15] A.G. Yodh, J. Golub, and T.W. Mossberg, Phys. Rev. A **32**, 844 (1985).

[16] R.M. Lowe and P. Hannaford, J. Phys. B **22**, 407 (1989).

[17] NiChrome V beaded heater from Cole-Parmer, Niles IL 60714.

[18] I.S. Grigoriev and E.Z. Meilikhov eds. *Handbook of Physical Quantities* (CRC Press, Boca Raton, 1997).

[19] We use 20 mW laser diodes from Semco Laser Technology, Baldwin Park CA, 91706.

[20] Starna Cells Inc., Atascadero CA, 93423.

[21] R.W. Berends and L. Maleki, J. Opt. Soc. Am B **9**, 332 (1992).

[22] H. Schuler, J. Roig, and H. Korsching, Z. Phys **111**, 165 (1938).

[23] J.S. Ross and K. Murakawa, J. Phys. Soc. Jpn. **19**, 249 (1964).

[24] J. Golub, Y.S. Bai, and T.W. Mossberg, Phys. Rev. A **37**, 119 (1988).

[25] E.L. Lewis, Physics Reports **58**, 1 (1980).

[26] I.B. Khriplovich, *Parity Nonconservation in Atomic Phenomena* (Gordon and Breach, Philadelphia, 1991).

[27] There are a number of efficient algorithms for numerical computation of the complex error function. We use algorithm 363 [W. Gautschi, Comm. of the ACM **12**, 635 (1969)].

[28] D.L. Clark, M.E. Cage, D.A. Lewis, and G.W. Greenlees, Phys. Rev. A **20**, 239 (1979).

[39] W.A. Wijngaarden and J. Li, J. Opt. Soc. Am. B **11**, 2163 (1994).

[30] J.H Broadhurst, M.E. Cage, D.L. Clark, G.W. Greenlees, J.A.R. Griffith, and G.R. Isaak, J. Phys. B **7**, L513 (1974).

[31] C.S. Wood, S.C. Bennett, D. Cho, B.P. Masterson, J.L. Roberts, C.E. Tanner, and C.E. Wieman, Science **275**, 1759 (1997).

[32] S.C. Haydon ed., *An Introduction to Discharge and Plasma Physics* (University of New England, Armidale, 1964).

[33] D. Budker, *WEIN-98 Conference Proceedings*, June 15-19, (1998); M.-A. Bouchiat and C. Bouchiat, *Rep. Prog. Phys.* **60**, 1351 (1997);